J Neuropathol Exp Neurol
Vol. 77, No. 4, 2018, pp. 282–295
doi: 10.1093/jnen/nly002

ORIGINAL ARTICLE

Intravenous Administration of a MTMR2-Encoding AAV Vector Ameliorates the Phenotype of Myotubular Myopathy in Mice

Nathalie Danièle, PhD, Christelle Moal, BS, Laura Julien, BS, Martina Marinello, PhD, Thibaud Jamet, PhD, Samia Martin, PhD, Alban Vignaud, PhD, Michael W. Lawlor, MD, PhD, and Ana Buj-Bello, MD, PhD

Abstract

X-linked myotubular myopathy (XLMTM) is a severe congenital disorder in male infants that leads to generalized skeletal muscle weakness and is frequently associated with fatal respiratory failure. XLMTM is caused by loss-of-function mutations in the *MTM1* gene, which encodes myotubularin, the founder member of a family of 15 homologous proteins in mammals. We recently demonstrated the therapeutic efficacy of intravenous delivery of rAAV vectors expressing MTM1 in animal models of myotubular myopathy. Here, we tested whether the closest homologues of MTM1, MTMR1, and MTMR2 (the latter being implicated in Charcot-Marie-Tooth neuropathy type 4B1) are functionally redundant and could represent a therapeutic target for XLMTM. Serotype 9 recombinant AAV vectors encoding either MTM1, MTMR1, or MTMR2 were injected into the tibialis anterior muscle of *Mtm1*-deficient knockout mice. Two weeks after vector delivery, a therapeutic effect was observed with *Mtm1* and *Mtmr2*, but not *Mtmr1*; with *Mtm1* being the most efficacious transgene. Furthermore, intravenous administration of a single dose of the rAAV9-*Mtmr2* vector in XLMTM mice improved the motor activity and muscle strength and prolonged survival throughout a 3-month study. These results indicate that strategies aiming at increasing MTMR2 expression levels in skeletal muscle may be beneficial in the treatment of myotubular myopathy.

Key Words: AAV vector, Mouse model, MTM1, MTMR1, MTMR2, Myotubular myopathy, Myotubularin.

INTRODUCTION

Centronuclear myopathies are a group of rare congenital skeletal muscle disorders classified together because of the presence of centrally localized nuclei within hypotrophic myofibers (1). The most severe and frequent form of these myopathies, X-linked myotubular myopathy (XLMTM, OMIM 310400) is a life-threatening disease affecting 1 in 50 000 male infants. XLMTM is characterized by severe hypotonia, generalized muscle weakness and respiratory failure at birth (2). Even though intensive care measures including ventilation and feeding support ameliorate the clinical status beyond the postnatal period, the disease is often fatal within the first years of life (2). Myotubular myopathy is a hereditary monogenic disease caused by loss-of-function mutations in the *MTM1* gene (3). Myotubularin, the encoded protein, is a phospholipid phosphatase that dephosphorylates the D3′ position of the inositol ring of phosphatidylinositol-3-phosphate (PI3P) and phosphatidylinositol-3, 5-bisphosphate [PI(3, 5)P2] (4–6). Although myotubularin is ubiquitously expressed (3), the pathology caused by its deficiency is mainly muscular. Myogenesis takes place, but muscle fibers are hypotrophic and weaker (7–10). They present profound structural abnormalities, such as mislocalization of nuclei and mitochondria (7–11), disruption of the intermediate filament network (12), triad disorganization (8–10, 13), and a reduction in the number and proliferation capacity of satellite cells (14). From a functional point of view, deficiencies in neuromuscular transmission (15, 16), excitation-contraction coupling (8, 9), and mitochondrial function (12) were previously suggested to account for muscle weakness and fatigability.

Although myotubular myopathy has no curative treatment in patients to date, several experimental therapies are currently being explored (15–20). We recently demonstrated that systemic AAV-mediated MTM1 gene therapy could

From INTEGRARE, INSERM UMRS 951, Univ Evry, Université Paris-Saclay, France (ND, CM, LJ, MM, TJ, ABB); R&D Department, Genethon, Evry, France (ND, CM, LJ, MM, TJ, SM, AV, ABB);Genethon, Evry, France (ND, CM, LJ, MM, TJ, SM, AV, ABB); and Division of Pediatric Pathology, Department of Pathology and Laboratory Medicine and Neuroscience Research Center, Medical College of Wisconsin, Milwaukee, Wisconsin (MWL).

Send correspondence to: Ana Buj Bello, MD, PhD, R&D Department, Genethon, INSERM U951, 1 bis rue de l'Internationale, 91000 Evry, France; E-mail: abujbello@genethon.fr

This study was supported by the AFM-Telethon, France, the National Institutes of Health (K08 AR059750), USA, and the ATIGE from the Genopole d'Evry, France.

Disclosures: Ana Buj-Bello is an inventor of 2 issued patents on MTM1 gene therapy for myotubular myopathy and a scientific advisor for Audentes Therapeutics. Michael W. Lawlor receives research funding support from Audentes Therapeutics, Solid Biosciences, and Demeter Therapeutics. Michael W. Lawlor is a member of the Scientific Advisory Board of Audentes Therapeutics and was recently a consultant for Sarepta Therapeutics.

Supplementary Data can be found at http://www.jnen.oxfordjournals.org.

largely improve the XLMTM phenotype and prolong survival in mouse and dog models of the disease (19, 21). Interestingly, myotubularin is the archetypical and founding member of a family of 15 homologous proteins, the myotubularin-related proteins (MTMR) (22). Like myotubularin, some MTMR proteins (MTMR1–4, MTMR6–8, MTMR14) display lipid phosphatase activity toward PI3P and PI(3, 5)P2 and contain the conserved $C(X)_5R$ active motif in the catalytic site, whereas others are inactive due to amino acid substitutions within this catalytical motif (MTMR5, MTMR9–13) (22). The MTMR proteins present some degree of functional redundancy (22, 23), suggesting that overexpression of a homologous protein might rescue myotubularin deficiency. This approach could define a novel molecular target for drug development in myotubular myopathy with the goal of increasing the expression level of the endogenous gene, or by exogenous delivery. Additionally, these proteins would offer alternative gene therapy strategies for situations where myotubularin replacement is not well tolerated (which may occur in patients who express no myotubularin protein). Amongst the MTMR proteins, myotubularin-related protein 1 (MTMR1) and 2 (MTMR2) appear as the most relevant for that application because the 2 proteins belong to the same phylogenetic subgroup than myotubularin (24); they share the highest level of structural similarity and display 3-phosphatase activity towards PI3P (4, 5, 23, 25–29) and PI(3, 5)P2 (6, 26, 28–30). In the present study, we compared the therapeutic effect of these candidates by gene transfer and demonstrate that intramuscular delivery of a rAAV9 vector encoding MTMR2 rescues the muscle pathology in a murine model of myotubular myopathy, while the benefit of MTMR1 overexpression remains only marginal. Furthermore, whole body treatment of *Mtm1* knockout (KO) mice by intravenous injection of a single dose of a serotype 9 recombinant adeno-associated viral vector (rAAV9) expressing the *Mtmr2* gene ameliorated muscle function and prolonged lifespan, indicating that MTMR2 can compensate myotubularin deficiency in skeletal muscle.

MATERIALS AND METHODS

Generation and Titration of Recombinant AAV Vectors

Murine *Mtmr1*, *Mtmr2*, and *Mtm1* coding sequences were cloned downstream of the human desmin promoter in an AAV2 plasmid backbone by PCR amplification. Pseudotyped recombinant rAAV2/9 (rAAV9) viral preparations were generated by packaging AAV2-inverted terminal repeat (ITR) recombinant genomes into AAV9 capsids. Briefly, the *cis*-acting plasmids encoding one of the transgenes pAAV2-Des-*Mtm1*, *-Mtmr1*, *or Mtmr2*, a trans-complementing rep-cap9 plasmid encoding the proteins necessary for the replication and structure of the vector and an adenovirus helper plasmid were cotransfected into HEK293 cells. Vector particles were purified through 2 sequential cesium chloride gradient ultracentrifugations and dialyzed against sterile phosphate-buffered saline (PBS). DNAse I resistant viral particles were treated with proteinase K. Viral titers were quantified by a TaqMan real-time PCR assay (Applied Biosystems, Foster City, CA), with primers and probes specific for the ITR2 region (31), and expressed as viral genomes per ml (vg/ml). The primer pairs and TaqMan MGB probes used for ITR2g amplification were: Forward 5′-CTCCATCACTAGGGGTTCCTTGTA-3′; reverse 5′-TGGCTACGTAGATAAGTAGCATGGC-3′; and MGB/taqman probe 5′-GTTAATGATTAACCC-3′.

Animal Care and Experimental Design

All mice were handled according to the European guidelines for the humane care and use of experimental animals and procedures were approved by the institutional ethical committee (number CE 12-006). The *Mtm1*-KO murine strain obtained by constitutive deletion of *Mtm1* exon 4 was previously described (7), and maintained in a 129SvPasIco background (9). Wild-type (WT) littermates were used as control animals. For the intramuscular administration study, a volume of 10 µl of rAAV9-*Mtmr1* (3×10^{10} vg per injection), rAAV9-*Mtmr2* (2.4×10^{10} vg), rAAV9-*Mtm1* (3×10^{10} vg), or PBS was injected into the tibialis anterior (TA) muscle of 2-week-old male KO animals. WT male littermates were treated with an equivalent volume of PBS. Two weeks after injection, TA muscles were sampled, quickly frozen in isopentane cooled with liquid nitrogen and stored at −80°C. For the intravenous administration, a dose of 2.4×10^{14} vg/kg of body weight of rAAV9-*Mtmr2* was injected in the tail vein of 2-week-old male KO animals. Age-matched WT animals received an equivalent volume of PBS. Analyses were performed 3 months after the injections. The number of animals in each experimental procedure and subgroup are included in the figure legends.

Quantitative RT-PCR

Total RNA was purified from whole TA muscles using TRIzol reagent (Life Technologies, Saint Aubin, France), according to the manufacturer's instructions. RNA concentration was determined by measure of the optical density at 260 nm and RNA integrity was confirmed by electrophoresis using an agarose gel containing GelRed as a nucleic acid stain (Biotium, Hayward, CA). Genomic DNA was degraded with a DNAse treatment (Thermo Scientific, Rockford, IL), and cDNA was synthesized from RNA using RevertAid H minus Reverse Transcriptase (Thermo Scientific, Waltham, MA) in the presence of Random Primers (Thermo Scientific). Real-time PCR was performed using SYBR green (Life Technologies) as a nucleic acid stain and an ABI Prism 7900 apparatus (Applied Biosystems). The primers used are: *Mtmr1* Forward 5′(GGCACAGATGGAAGAAGCTC)3′, reverse 5′ (CCACT CTGCTGATCACTCCA)′; *Mtmr2* Forward 5′(TGCTGAC AAGGTCGAGTCTG)3′, reverse 5′(CTGCGTCAGCATGG TTCTTA)3′; *Chrn-α1* Forward 5′(GAATCCAGATGACTAT GGAG)3′, reverse 5′(GACAATGATCTCACAGTAGC)3′; *Chrn-δ* Forward 5′(AACGTGTGGATAGATCATGC)3′, reverse 5′(CATAGACAAGCACATTGCAGG)3′; *Chrn-γ* Forward 5′(ATCCGGCACCGACCGGCTAA)3′, reverse 5′(CATTTCTGCCCGCCCGCCTT)3′. The ubiquitous acidic ribosomal phosphoprotein P0 (*Rplp0*) was used to normalize the data across samples, and primers are: Forward 5′(CTCC

AAGCAGATGCAGCAGA)3′, reverse 5′(ATAGCCTTGCG CATCATGG)3′.

Western Blot

For intramuscular administration studies, thirty micrometer of muscle cryo-sections were sliced and proteins were extracted using 50 µl of a lysis buffer containing 10 mM Tris HCl pH 7.4, 150 mM NaCl, 5 mM EGTA, 2 mM sodium orthovanadate, 100 mM NaF, 4 Mm Na pyrophosphate, 1% Triton X-100, 0.5% IGEPAL, and Protease Inhibitor Cocktail used according to the manufacturer's instruction (Roche Applied Science, Meylan, France). For intravenous administration studies, muscle proteins were extracted in the same buffer with a ratio of 200 µl per 30 mg of frozen muscle and homogenized with a FastPrep-24 sample preparation system (MP Biomedicals, Illkirch, France). In each case, samples were incubated on ice with occasional mixing for 30 minutes. After centrifugation at 12 000*g* for 10 minutes at 4°C, the supernatants were recovered for Western blot analysis. Total protein concentration was determined by the Bradford methodology according to the manufacturer's instruction (BioRad, Marnes-la-Coquette, France). Fifty to 80 µg of total proteins were denatured for 5 minutes at 95°C in a buffer containing 125 mM Tris HCl pH 6.8, 4% SDS, 0.2 M DTT, 50% glycerol, and bromophenol blue. Protein samples were submitted to sodium dodecyl sulfate-polyacrylamide gel electrophoresis in 10% acrylamide gels and transferred onto PVDF membranes (GE Healthcare, Aulnay-Sous-Bois, France) by the application of an electric field (100 V, 1 hour) at 4°C. The membranes were first incubated for 60 minutes at room temperature in a blocking solution composed of 50% Tris-buffered saline (TBS), 0.1% Tween 20, and 50% Odyssey blocking buffer (LI-COR, Lincoln, NE) and then probed successively with a custom-made rabbit polyclonal antibody raised against the C-terminal extremity of murine MTMR1 (peptide CGSSPTHSATPVHTSV), MTMR2 (peptide CASS-PAQCVTPVQTVV), and MTM1 (17) (all used at a dilution of 1:2000), and a mouse monoclonal antibody specific for α-tubulin (dilution 1:2000; Millipore, Billerica, MA). Antibody incubations were carried out for 60 minutes at room temperature or overnight at 4°C in TBS, 0.1% Tween 20, and 1% milk. Detection was performed with a secondary goat antirabbit antibody coupled to IRDye 800 nm (dilution 1:10 000; LI-COR) for MTMR1, MTMR2 and MTM1, and with a secondary goat antimouse antibody coupled to AlexaFluor 680 nm (dilution 1:10 000; Life Technologies) for α-tubulin and the membranes were exposed to the Odyssey infrared imaging system (LI-COR) for detection and quantification of the fluorescent signal (Odyssey software, version 1.2, 2003).

Measurement of PI3P Level

In intramuscular studies, the level of PI3P was measured by immuno-staining on 8-µm-thick TA slices. The tissue was fixed for 20 minutes at -20°C in cold acetone and epitopes were retrieved by boiling the sections for 10 minutes in PBS. After 15-minute permeabilization in 0.1% Triton in TBS, unspecific sites were blocked by incubating the sections for 45 minutes at 37°C in 10% donkey serum diluted in 0.1% Triton in TBS. PI3P staining was performed with a PI3P-specific mouse monoclonal antibody (1:250 in 0.1% Triton in TBS; Echelon Biosciences Incorporated, Salt Lake City, UT) for 1 hour at 37°C. After TBS washes, the sections were incubated 2 hours at room temperature with an Alexa Fluor 594-conjugated goat antimouse antibody (1:500 in TBS; Life Technologies), glass slides were mounted with Fluoromount reagent (SouthernBiotech, Birmingham, AL); the staining was visualized with a 63× 1.4NA immersion objective on a Leica confocal microscope TCS-SP2 (Leica Microsystems GmbH, Wetzlar, Germany). On 4 randomly selected fields, intracellular subsarcolemmal regions of interest (ROIs) were manually drawn inside 10 representative fibers and the mean value of pixel intensity measured using ImageJ (Rasband, W.S., ImageJ, U. S. National Institutes of Health, Bethesda, MD, https://imagej.nih.gov/ij/, 1997–2016).

In intravenous studies, lipids were extracted from whole soleus muscles and PI3P was measured using a proprietary PI3P-specific ELISA method (Echelon Biosciences, Inc.). Briefly, frozen soleus were powdered and incubated in 150 µl of Western blot lysis buffer for 45 minutes at 4°C. Lipids were extracted by the addition of 900 µl of a chloroform/methanol/0.1 M HCl mixture (1/1/1). After vigorous shaking, the lower organic phase was separated by a 2-minute 10 000*g* centrifugation, sampled, and a second extraction carried out with the addition of 240 µl of methanol/1 M HCl mix (1/1). After settling, the lower phase was dried using a speed-vac concentrator system (Thermo Fisher Scientific, Villebon Sur Yvette, France), and kept at -80°C until resuspension and PI3P assay according to the manufacturer's instructions.

Histology, Morphometry, and Immuno-Stainings

Histology and Morphometry

Serial 8-µm-thick transverse cryo-sections were prepared from frozen muscles. Hematoxylin and eosin (H&E) staining was performed using standard procedures. The proportion of internalized nuclei was quantified from H&E-stained sections using the Histolab software (Microvision, Evry, France).

Nicotinamide adenine dinucleotide tetrazolium reductase (NADH-TR) coloration was performed in order to visualize the localization of mitochondria and endoplasmic reticulum. Muscle cryo-sections were incubated for 10 minutes at 57°C in a solution composed of 50 mM Tris HCl, pH 7.3, 1.2 mM Nitroblue Tetrazolium (Sigma-Aldrich, Lyon, France) and 0.6 mM β-NADH (Sigma-Aldrich), washed, and mounted in Eukitt (Sigma-Aldrich).

For determination of the number and minimal diameter of fibers, laminin immunostaining (antibody) was performed to outline each fiber. Briefly, endogenous peroxidases were neutralized by incubation in H_2O_2 for 30 minutes. Sections were incubated for 30 minutes with 10% goat serum in PBS (DAKO, Trappes, France) in order to block unspecific sites and then overnight in a 1:1000 dilution of antilaminin rabbit polyclonal antibody (DAKO) at room temperature. After PBS

washes, sections were incubated with a goat antirabbit secondary antibody conjugated with horseradish peroxidase (Kit En Vision Rabbit HRP, DAKO) for 30 minutes at room temperature, and the revelation was performed after additional PBS washes by incubation in 3, 3′-diaminobenzidine (DAB) for 2 minutes. Myofibers minor diameters were automatically measured on digital images of the sections using the Ellix software (Microvision).

Pax 7 Immunostaining

Pax 7 immunostaining was performed on sections of TA muscles fixed 5 minutes in 4% paraformaldehyde (PFA) in PBS, permeated 6 minutes in methanol at -20°C and treated for protein refolding in citric acid at 100°C for 10 minutes. Endogenous peroxidases were inhibited, and nonspecific sites were blocked using 5% BSA for 2 hours and Mouse-On-Mouse ([MOM], Vector Laboratories, Burlingame, CA) blocking reagent for 30 minutes. Sections were incubated overnight in murine antibodies specific for Pax7 (DSHB, Iowa City, IA; dilution 1:20 in 4% BSA in PBS), and 45 minutes in biotinylated goat antimouse antibodies (1:1000 in 4% BSA in PBS; SouthernBiotech). Biotin was revealed using the peroxidase-conjugated Vectastain system (Vectastain ABC system, Vector Laboratories) and its DAB substrate. Muscle sections were counterstained with eosin, mounted and pax7-positive fibers were quantified with the Histolab software.

Immunofluorescence

Transverse muscle sections were fixed for 10 minutes by incubation either in PBS at 100°C for the dihydropyridin receptor alpha (DHPRα1) staining or for 7 minutes in 4% PFA in PBS at 4°C for the ryanodine receptor 1 (Ryr1) and desmin staining, respectively. Nonspecific antigens were blocked at room temperature for 1 hour with PBS containing either 3% bovine serum albumin (DHPRα1 and desmin detection) or MOM blocking reagent (Ryr1 detection). Sections were incubated in mouse primary monoclonal antibodies directed against DHPRα1 (dilution 1:400, overnight at 4°C; Thermo Scientific) or Ryr1 (dilution 1:100, 1 hour at room temperature; Abcam, Cambridge, MA) or in goat polyclonal antibodies specific for desmin (1:100, 1 hour at room temperature; Santa Cruz Biotechnology, Heidelberg, Germany). After extensive PBS washes, sections were incubated with donkey antigoat antibodies conjugated with Alexa Fluor 488 (dilution 1:1000; Life Technologies) for desmin staining, or with biotinylated goat antimouse antibodies (dilution 1:200; SouthernBiotech) and, after additional washes, with Alexa Fluor 488-bound streptavidin (1:1000; Life Technologies) for DHPRα1 and Ryr1 stainings, respectively. Glass slides were mounted with FluorSave reagent (Calbiochem, Merck Millipore, Darmstadt, Germany) and visualized with a Leica confocal microscope TCS-SP2 (Leica Microsystems GmbH).

Electron Microscopy

Electron microscopy was performed as previously described (9, 18) for the evaluation of sarcotubular architecture. Briefly, glutaraldehyde fixed skeletal muscle specimens were processed at the Medical College of Wisconsin (MCW) EM Core facility for the evaluation of triad morphology. After confirming appropriate tissue quality on scout sections, longitudinally oriented 30-nm sections were stained with 2% uranyl acetate and Reynold's lead citrate, and electron microscopy was performed using a Hitachi H600 transmission electron microscope. Longitudinally oriented muscle fibers were evaluated and photographed, with photography of the single best-oriented region from each myofiber in the specimen at 10 000×, 20 000×, and 30 000× magnification. Ten fibers per specimen were evaluated and photographed in this manner. The number of transverse (T)-tubules, longitudinal (L)-tubules, and triad structures were then manually quantified by a blinded, board-certified neuropathologist using the 20 000× magnification image. The values for all images in a given treatment condition were pooled together to generate average numbers of T-tubules, L-tubules and triads in that condition.

Measurement of Muscle Function

Actimeter Test

Murine spontaneous locomotor activity was measured with the LE 8811 IR motor activity monitor (Bioseb, Chaville, France). Briefly, mice were placed in an open field bounded with 16 × 16 horizontal photoelectric Infrared beams able to measure 3-dimensional movements of the animals. The field is shielded from external noise and light, illuminated with a white fluorescent light and fully ventilated. The distance crossed was recorded for the 90 minute-course of the test.

Escape Test

The global strength of mice was evaluated by the "escape test" (32). Briefly, mice were placed on a platform facing the entrance of a 30-cm-long tube. A cuff wrapped around the tail was connected to a fixed force transducer and the mice were induced to escape within the tube in the direction opposite from the force transducer by a gentle pinching of the tail. A short peak of force was induced by this flight forward and the average of the 5 highest force peaks normalized by body weight were analyzed.

EDL Contractile Force

Measurements of isometric contractile properties of extensor digitorum longus (EDL) were performed in vitro according to methods previously detailed (33). Animals were anesthetized by intraperitoneal injection of pentobarbital (50 mg/kg). EDLs were surgically excised and soaked in an oxygenated Krebs solution (95% O_2 and 5% CO_2) containing 118 mM NaCl, 25 mM $NaHCO_3$, 5 mM KCl, 1 mM KH_2PO_4, 2.5 mM $CaCl_2$, 1 mM $MgSO_4$, and 5 mM glucose maintained at a temperature of 20°C. Muscles were connected at one end to an electromagnetic puller and at the other end to a force transducer, and stimulation was delivered through electrodes running parallel to the muscle. Twitch and tetanic (125 Hz, 300 mseconds) isometric contractions were recorded at Lo (the length at which maximal tetanic isometric force is

observed). For comparative purposes, normalized isometric force was assessed. Isometric tension was calculated by dividing the force by the estimated cross-sectional area of the muscle.

TA Contractile Force

Skeletal muscle function was evaluated by the measure of muscle contraction in situ, as previously described (34). Animals were anesthetized by intraperitoneal injection of Ketamine (100 mg/kg) and Xylazine (10 mg/kg) and supplemental doses were administered as required to maintain deep anesthesia. The knee and foot were fixed with clamps and stainless steel pins. The TA muscle was exposed and the distal tendon was cut and attached to a force transducer (Aurora Scientific, Dublin, Ireland). The sciatic nerves were proximally crushed and distally stimulated by a bipolar silver electrode using supramaximal square wave pulses of 0.1 msecond duration. Absolute maximal forces were determined at optimal length (length at which maximal tetanic tension was observed). The specific maximal force was calculated by normalizing the total muscle force with the muscle mass.

Statistical Analysis

Data are presented as means ± SE. Data were analyzed for normality using the Kolmodorov-Smirnov test and individual means were compared using the student parametric test or the Mann-Whitney nonparametric test. Differences were considered to be statistically significant at $p < 0.05$, $p < 0.01$, and $p < 0.001$.

Video

A video showing mice 3 weeks after intravenous injection of rAAV9-*Mtmr2* is included as Supplementary Data: WT mouse, untreated *Mtm1*-KO mouse (KO + PBS), and rAAV9-*Mtmr2*-treated *Mtm1*-KO mouse (KO + AAV).

RESULTS

Effect of *Mtmr1* and *Mtmr2* Gene Delivery in the Skeletal Muscle of *Mtm1*-KO Mice

In order to test whether overexpression of MTMR1 and MTMR2 proteins could rescue the pathological signs of myotubular myopathy, rAAV9 vectors carrying either *Mtmr1* (3×10^{10} viral genomes [vg]) or *Mtmr2* (2.4×10^{10} vg) were injected into the TA muscle of 2-week-old *Mtm1*-KO mice (see viral titration data in Supplementary Data Fig. S1A). A vector encoding myotubularin (3×10^{10} vg/TA) was used as a positive control, as we previously showed the efficiency of this transgene in correcting the XLMTM phenotype (17, 19). PBS was administrated in the contralateral muscle of KO animals and WT littermates as additional controls. At the time of treatment, the mRNA levels of *Mtmr1* and *Mtmr2* did not show significant changes in *Mtm1* KO muscles (Supplementary Data Fig. S2). Two weeks after vector injection, the mice were killed and TA muscles were sampled, weighed and processed for analyses. The vector copy number (viral genomes per diploid genome) in injected muscles was nearly identical amongst the various treatment conditions (4–6 vector copies, Supplementary Data Fig. S1B), and MTMR1 and MTMR2 protein levels, although undetectable in WT-PBS and KO-PBS TA, were strongly increased in AAV-treated KO muscles (Fig. 1A).

The histopathological signs of the disease were already present in myotubularin-deficient mice at the time of vector administration (9), and became more pronounced when mice were 4 weeks of age, as evidenced by an ~55% reduction of TA muscle weight (Fig. 1B). Expression of *Mtmr1*, *Mtmr2*, and *Mtm1* transgenes resulted in an increase of muscle weight 2 weeks after vector injection (+14.4% for *Mtmr1*, +18.5% for *Mtmr2*, +86.7% for *Mtm1*, Fig. 1B). Detailed morphometric analysis of *Mtmr1*-treated muscles showed a small but significant increase in myofiber mean diameter (15.3 µm in rAAV9-*Mtmr1* vs 13.5 µm in PBS-injected KO TA, $p < 0.05$), whereas the number of large fibers (diameter > 20 µm) remained unchanged (Fig. 1C). On the contrary, MTMR2 overexpression resulted in an increase in both muscle fiber diameter (mean 16.6 µm, i.e. +23%), and the amount of large myofibers (35% of fibers in rAAV9-*Mtmr2* vs 15% in PBS-injected TA), and was therefore more efficient than MTMR1 in compensating myotubularin deficiency.

MTMR2 but Not MTMR1 Restores PI3P Levels in Myotubularin-Deficient Muscle

Increased levels of PI3P in muscle were shown to play a critical role in the pathogenesis of XLMTM, as normalization by pharmacological inhibition of phosphatidylinositol 3-kinase resulted in histopathological amelioration and prolonged survival of *Mtm1*-KO mice (35, 36). We therefore quantified the level of this phosphoinositide in TA muscle 2 weeks after the injection of either PBS or the *Mtmr1*, *Mtmr2*, or *Mtm1* transgenes to see if vector response correlated with changes in PI3P levels. As already reported (8), the amount of PI3P was significantly increased in *Mtm1*-KO muscles (2.1-fold over WT-PBS values, $p < 0.01$; Fig. 1D). Interestingly, both *Mtmr2* and *Mtm1* gene transfer normalized PI3P levels in mutant muscle, whereas *Mtmr1* overexpression had no significant effect (2.6-fold over WT-PBS level, $p < 0.05$). These results suggest that exogenous MTMR1 is inefficient in dephosphorylating critical PI3P subpools in muscle whereas MTMR2 is able to cross-correct myotubularin enzymatic deficiency in vivo.

MTMR2 Overexpression Ameliorates the Internal Architecture of Muscle Fibers in *Mtm1*-KO Mice

To evaluate the effect of the treatment on other histopathological hallmarks of the disease further, H&E, NADH-TR, and immunofluorescence stainings were carried out on TA cross-sections of 4-week-old *Mtm1* mutant mice. In addition to hypotrophy, mutant muscle fibers contain internal nuclei and altered organization of intermyofibrillar mitochondria and endoplasmic reticulum, which accumulate in central areas or in the subsarcolemmal region (Fig. 2A) (37). Despite the

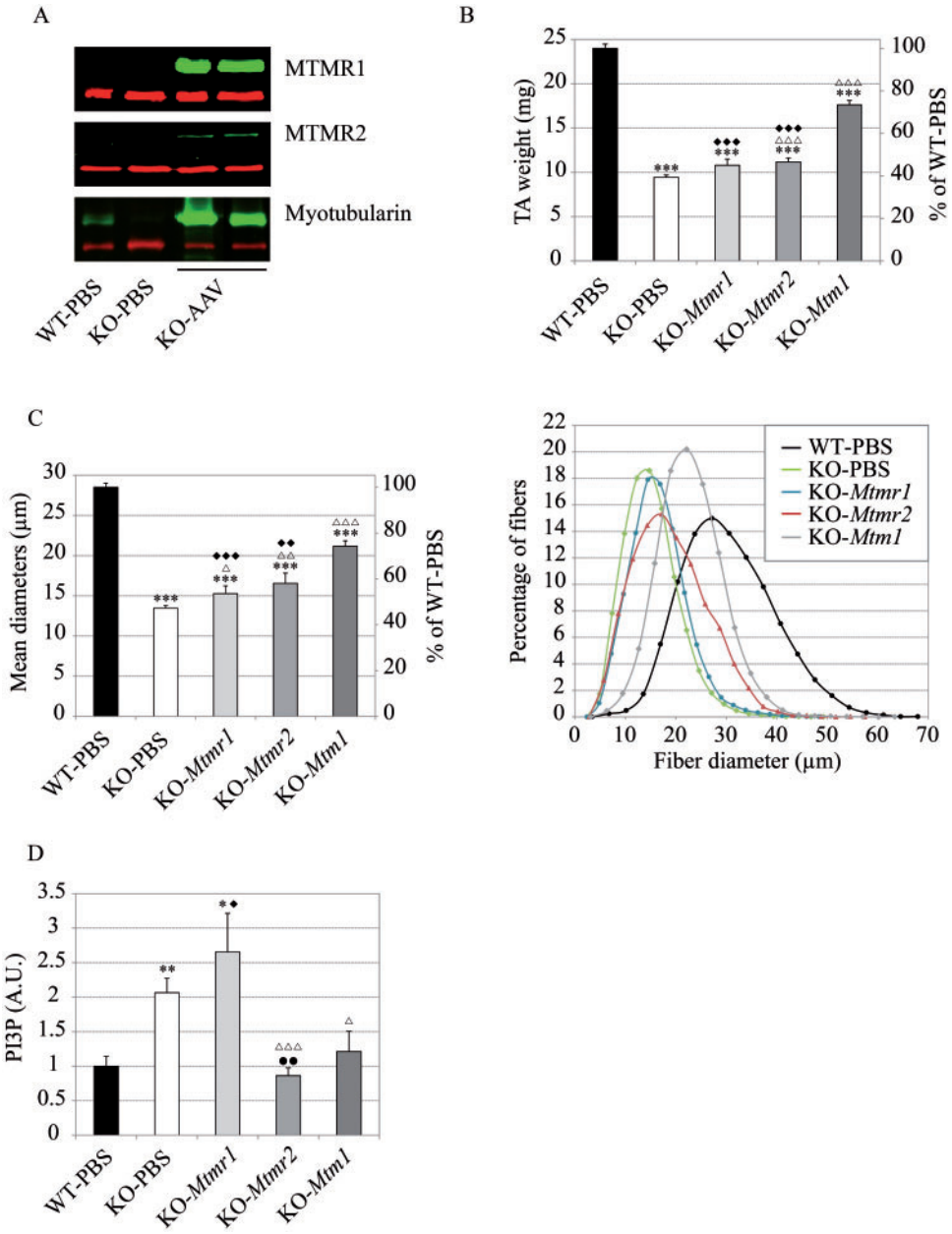

FIGURE 1. Effect of intramuscular rAAV9-mediated *Mtmr1* and *Mtmr2* gene transfer in *Mtm1* knockout mice. **(A)** Representative immunoblots of MTMR1 (top panel), MTMR2 (middle panel) and myotubularin (lower panel) protein levels (in green) in tibialis anterior of untreated (KO-PBS) and AAV-treated (KO-AAV) *Mtm1*-KO mice, and in saline-injected control muscle (WT-PBS). The immunodetection of α-tubulin was used as loading control (in red). **(B)** Weight of TA muscle from mutant mice 2 weeks after intramuscular delivery of rAAV9-*Mtmr1*, -*Mtmr2* or -*Mtm1*, and appropriate controls (KO-PBS and WT-PBS). Results are also shown as a percentage of WT values (WT-PBS n = 41; KO-PBS n = 44; KO-*Mtmr1* n = 8; KO-*Mtmr2* n = 22; KO-*Mtm1* n = 16). **(C)** Mean diameter of myofibers in PBS-, *Mtmr1*-, *Mtmr2*-, and *Mtm1*-injected tibialis anterior muscle (WT-PBS n = 13; KO-PBS n = 33; KO-*Mtmr1* n = 7; KO-*Mtmr2* n = 9; KO-*Mtm1* n = 8). ***, $p < 0.001$ versus WT-PBS; $^{\Delta}$, $^{\Delta\Delta}$, $^{\Delta\Delta\Delta}$, $p < 0.05$, 0.01, or 0.001 versus KO-PBS; $^{\blacklozenge\blacklozenge}$, $^{\blacklozenge\blacklozenge\blacklozenge}$, $p < 0.01$ or 0.001 versus KO-*Mtm1*. **(D)** PI3P level in TA muscles, A.U. arbitrary unit (WT-PBS n = 6; KO-PBS n = 5; KO-*Mtmr1* n = 5; KO-*Mtmr2* n = 6; KO-*Mtm1* n = 6). *, **, ***, $p < 0.05$, 0.01 or 0.01 versus WT-PBS; $^{\Delta}$, $^{\Delta\Delta\Delta}$, $p < 0.05$ or 0.001 versus KO-PBS; $^{\bullet\bullet}$, $p < 0.01$ versus KO-*Mtmr1*; $^{\blacklozenge}$, $p < 0.05$ versus KO-*Mtm1*.

presence of occasional internal nuclei, the architecture of myotubularin-deficient myofibers was largely ameliorated after AAV-mediated *Mtmr2* gene transfer, whereas it remained unchanged by *Mtmr1* overexpression. The percentage of fibers presenting internal nuclei, which was increased in PBS-injected KO TA (5.9-fold over WT-PBS values, $p < 0.001$), was equally reduced in presence of either MTMR2 or myotubularin 2 weeks after vector injection (respective diminution

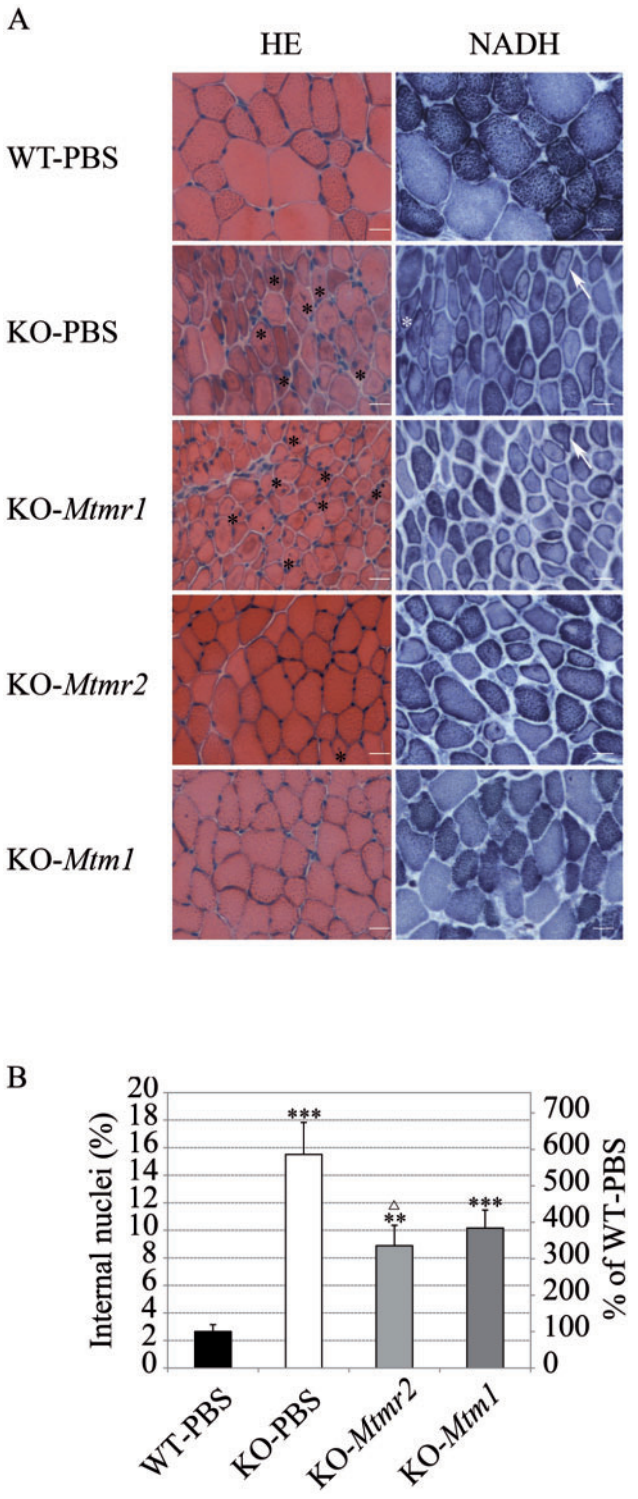

FIGURE 2. MTMR2 but not MTMR1 overexpression improves the histopathological features of myotubularin-deficient muscle. **(A)** H&E and NADH-TR stainings of TA cross-sections from *Mtm1*-KO and WT mice 2 weeks after intramuscular delivery of PBS or rAAV9 vectors carrying either *Mtmr1*, *Mtmr2*, or *Mtm1* transgenes. Nuclei internalization: Black stars on H&E; cytoplasmic and sub-sarcolemmal accumulations of mitochondria: White star and white arrow on NADH-TR staining, respectively. Scale bar = 20 μm. **(B)** Quantification of the percentage of myofibers containing internalized nuclei after rAAV9-*Mtmr2* and rAAV9-*Mtm1* treatment, and appropriate untreated controls. (WT-PBS n = 6; KO-PBS n = 13; KO-*Mtmr2* n = 9; KO-*Mtm1* n = 8). **, ***, $p < 0.01$ or 0.001 versus WT-PBS; $^{\Delta}$, $p < 0.05$ versus KO-PBS.

of 43% with MTMR2 and 35% with myotubularin; Fig. 2B). Given the absence of substantial therapeutic benefit from MTMR1 overexpression in *Mtm1*-KO muscles, only rAAV9-*Mtmr2*-treated muscles were further analyzed.

Other distinctive features of myotubularin deficiency in skeletal muscle fibers include aberrant localization of 2 triadic proteins, the DHPR1α (T-tubule marker) and the Ryr1 (junctional sarcoplasmic reticulum marker), and desmin, an intermediate filament protein interacting with MTM1 (9, 12). These proteins were abnormally distributed within the sarcoplasm and subsarcolemmal region in *Mtm1*-KO myofibers (Fig. 3A). AAV-mediated MTMR2 or myotubularin expression restored normal localization of DHPR1α, RYR1, and desmin with comparable efficacies, suggesting restructuring of the sarcotubular and intermediate filament networks.

In murine models of myotubular myopathy, the muscle pathology has also been linked to defects in the morphology and function of the neuromuscular junction (16) and in satellite cells (14), leading to alterations in the expression of several biomarkers such as various subunits of the acetylcholine receptor (AChR) and Pax7. In our experiments, we found that MTMR2 overexpression did not correct the increase in AChR subunit α1 (Chrn-α1), γ (Chrn-γ), and δ (Chrn-δ) mRNA levels observed in the contralateral KO-PBS muscle, while myotubularin did (Fig. 3B). With regards to the reported deficiency in muscle progenitor cells, we quantified the number of Pax7-positive cells in AAV-treated and untreated TA muscles, and found a significant partial restoration of this biomarker after expression of either *Mtmr2* or *Mtm1* transgene (2- and 6.7-fold increase of satellite cells in MTMR2 and myotubularin-treated muscles, $p < 0.01$ and $p < 0.001$, respectively; Fig. 3C). Finally, we quantified the number of triads, transverse (T)-tubules, and longitudinal (L)-tubules in muscle preparations (Supplementary Data Fig. S3). Among these parameters, we found that the amount of L-tubules in rAAV9-*Mtmr2*-treated TA, which is significantly increased in KO-PBS animals as previously described (9), was decreased. The findings suggest a partial improvement of the sarcotubular architecture, but should be interpreted cautiously because the T-tubule and triad numbers did not significantly improve.

Altogether, these results show that MTMR2 overexpression in myotubularin-deficient skeletal muscle ameliorates pathological and molecular signs of the disease, even though less efficiently than MTM1 itself.

Mtmr2 Gene Transfer Increases Muscle Strength in *Mtm1*-Deficient Muscles

XLMTM mice display progressive muscle weakness starting in the hind limbs at early phases of the disease (7, 9). Indeed, the total and specific tetanic forces of TA muscle

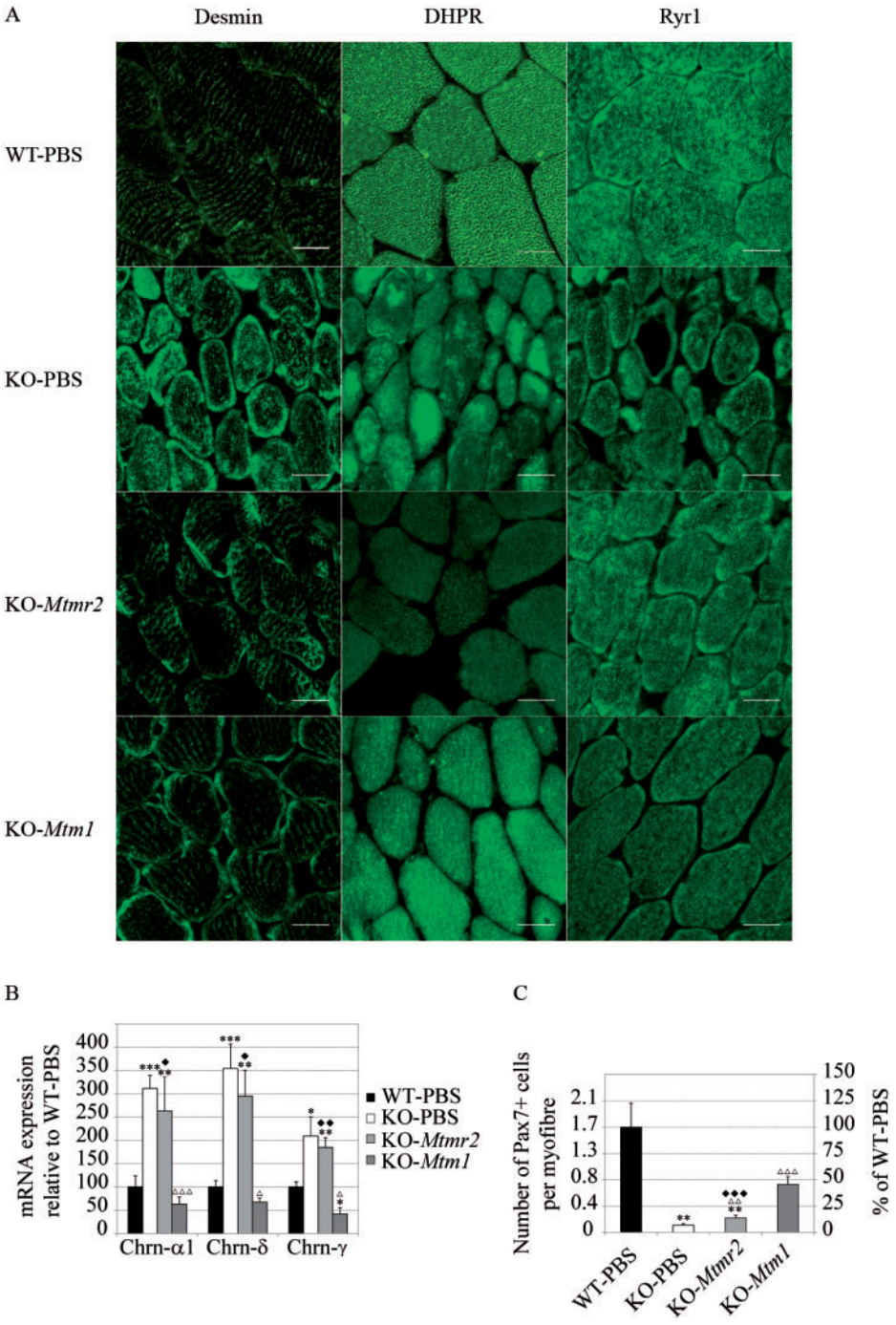

FIGURE 3. Restoration of XLMTM muscle biomarkers by *Mtmr2* gene transfer. **(A)** Localization of desmin (left panels), DHPR1α (middle panels), and Ryr1 (right panels) proteins in tibialis anterior cross sections from *Mtm1*-KO and WT mice 2 weeks after intramuscular delivery of either rAAV9-*Mtmr2*, rAAV9-*Mtm1*, or saline. Scale bar = 20 μm. **(B)** Transcript levels of AChR subunits (Chrn-α1, Chrn-δ, and Chrn-γ) in untreated and AAV-treated TA muscle (WT-PBS n = 7; KO-PBS n = 8; KO-*Mtmr2* n = 8; KO-*Mtm1* n = 3). **(C)** The number of Pax7-positive cells per myofiber was quantified in TA of wild-type and *Mtm1*-KO mice 2 weeks after PBS, rAAV9-*Mtmr2* or rAAV9-*Mtm1* administration (WT-PBS n = 10; KO-PBS n = 9; KO-*Mtmr2* n = 9; KO-*Mtm1* n = 5). *, **, ***, $p < 0.05$, 0.01 or 0.001 versus WT-PBS; $^{\Delta}$, $^{\Delta\Delta}$, $^{\Delta\Delta\Delta}$, $p < 0.05$, 0.01 or 0.001 versus KO-PBS; $^{\blacklozenge}$, $^{\blacklozenge\blacklozenge}$, $^{\blacklozenge\blacklozenge\blacklozenge}$, $p < 0.05$, 0.01 or 0.001 versus KO-*Mtm1*.

dropped significantly in 4-week-old *Mtm1*-KO mice by 90% and 80%, respectively, versus the WT animals ($p < 0.001$, Fig. 4). We quantified the effect of transgene expression in the strength of TA muscle 2 weeks after vector injection. MTMR2 overexpression led to a 2.9- and 2.5-fold increase in the total and specific forces, respectively, with respect to values in KO-

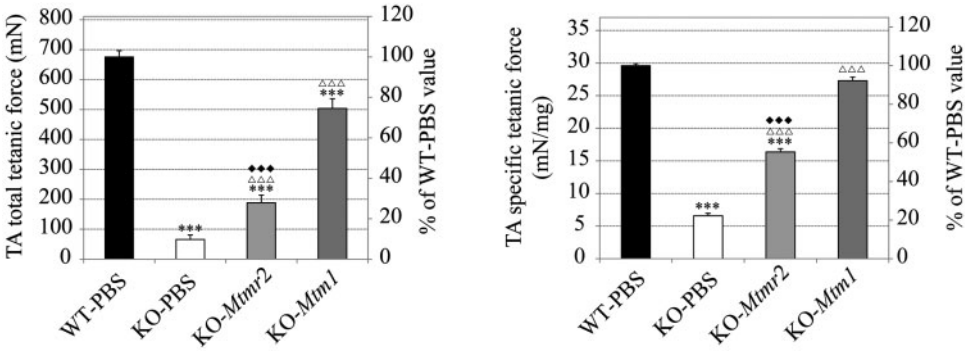

FIGURE 4. Intramuscular delivery of rAAV9-*Mtmr2* increases muscle strength in *Mtm1*-KO mice. Total tetanic (left graph) and specific (right graph) force of TA muscle from KO mice after intramuscular delivery rAAV9-*Mtmr2* and -*Mtm1* vectors, and appropriate controls (WT-PBS n = 16; KO-PBS n = 10; KO-*Mtmr2* n = 10; KO-*Mtm1* n = 7). ***, $p < 0.001$ versus WT-PBS; $^{\Delta\Delta\Delta}$, $p < 0.001$ versus KO-PBS; $^{\blacklozenge\blacklozenge\blacklozenge}$, $p < 0.001$ versus KO-*Mtm1*.

PBS muscles (Fig. 4). Albeit partial compared to myotubularin replacement, the effect of MTMR2 on the specific force clearly showed an improvement of the contractile quality of *Mtm1*-KO myofibers.

Systemic Delivery of rAAV9-*Mtmr2* Prolongs Survival and Improves Muscle Function of XLMTM Mice

Myotubularin-deficient mice survive on average less than 2 months (median survival 51 days; Fig. 5A). We therefore assessed the efficacy of rAAV9-*Mtmr2* treatment at the whole body level of mutant mice over a 3-month observation period. We first tested an intravenous dose of 8×10^{13} vg/kg, which is close to the efficacious dose of rAAV8-*Mtm1* that was administrated in our previous gene replacement study in XLMTM mice (15), but did not observe a therapeutic benefit (not shown). We therefore increased the dose of rAAV9-*Mtmr2* and injected 2.4×10^{14} vg/kg of vector into the tail-vein in *Mtm1*-KO mice at 2 weeks of age. All mutant mice treated at this higher dose remained viable and gained body mass during the study period (Fig. 5A, B and Supplementary Data Video). At the time of death, transgene expression was analyzed at the mRNA and protein level in a panel of representative muscles throughout the body (Fig. 5C, D). *Mtmr2* mRNA expression was 50–100 times higher than the endogenous level in skeletal muscles (Fig. 5C), reaching a 250-fold increase in heart (Supplementary Data Fig. S4), and resulted in high levels of MTMR2 protein in transduced muscles (Fig. 5D). We also analyzed PI3P levels in skeletal muscle and, similar to the effect observed after local delivery of rAAV9-*Mtmr2* in mutant muscle (Fig. 1D), systemic administration of this vector reduced PI3P levels in *Mtm1*-deficient muscle 7 weeks after vector injection (Fig. 5E).

All analyzed skeletal muscles from vector-treated mice gained weight compared to untreated mutant mice at 5 weeks of age, consistent with the overall increase of body weight (Fig. 6A). This amelioration correlated with an increase in myofiber size (mean diameter was 15.9 µm in TA and 17 µm in biceps brachii of 5-week-old *Mtm1*-KO animals vs 31.9 µm and 27.4 µm, respectively, 3 months after vector injection), and a quasi-normalization in mitochondrial and nuclear distribution within myofibers (Fig. 6B–D). In the hearts of rAAV9-*Mtmr2*-treated KO mice, we found small focal patches of fibrosis generally associated with cellular infiltrates, lesions that were clinically well-tolerated (Supplementary Data Fig. S4).

To assess whether *Mtmr2* gene therapy ameliorates the excitation-contraction coupling machinery in *Mtm1*-KO animals, the number of triads and the morphology of tubules (transverse -T- or longitudinal -L-) were quantified in TA samples 7 weeks after vector injection. Our results show that the abnormal reduction of triads and presence of L-tubules that are observed in myotubularin-deficient muscle were both largely corrected by systemic administration of the rAAV9-*Mtmr2* vector (7 triads per ROI with 5% of L-tubules in KO-PBS TA vs 11.1 triads per ROI with 1% of L-tubules in KO-*Mtmr2* muscle), consistent with a partial restoration of the triad architecture in skeletal muscles upon treatment (Fig. 6E).

Finally, to measure the effect of gene therapy on global muscle function, the open field actimeter and escape tests were used. Mutant mice were very weak (whole body tension, 0.07 ± 0.01 vs 0.15 ± 0.005 N/g in healthy animals) and covered less than half the distance explored by WT littermates at 5 weeks of age (Fig. 7A, B). Importantly, mice treated with rAAV9-*Mtmr2* had a significant improvement in muscle function with values close to normal at 3 months postinjection (86% recovery of whole body strength, 0.16 ± 0.02 N/g). Accordingly, the specific tetanic force of isolated EDL (Fig. 7C) and soleus (data not shown), muscles was almost normalized 3 months after treatment. Altogether, our results demonstrate that the reduced lifespan and muscle impairment associated with myotubularin deficiency in mice can be rescued by systemic administration of a vector expressing the homologous MTMR2 protein.

DISCUSSION

In the present study, we investigated the potency of both MTMR1 and MTMR2 to compensate myotubularin deficiency in skeletal muscle and demonstrate that only rAAV9-mediated expression of MTMR2 led to major improvements

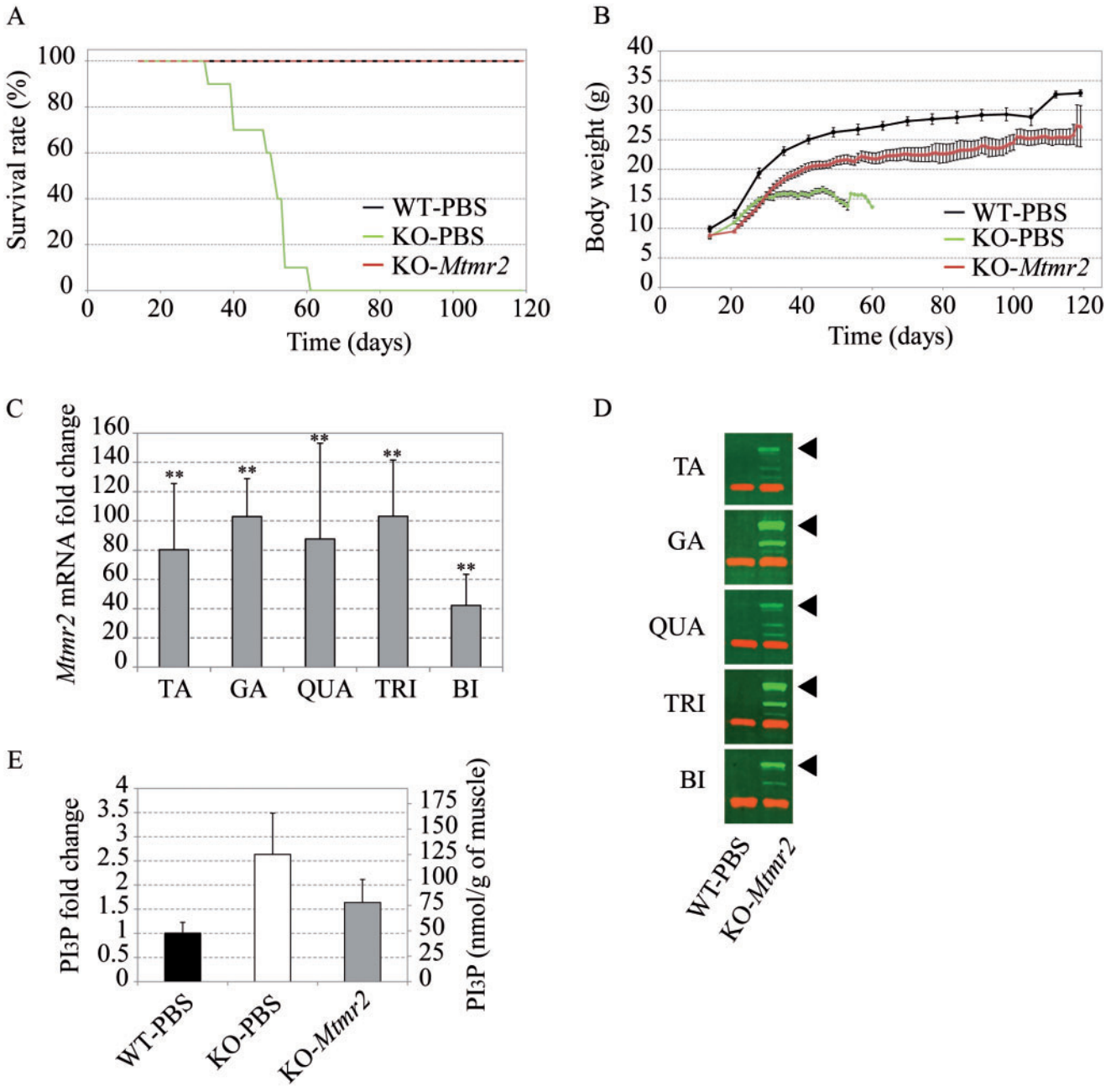

FIGURE 5. Intravenous administration of rAAV9-*Mtmr2* results in muscular MTMR2 overexpression and prolongs the lifespan of myotubularin-deficient mice. **(A, B)** Effect of intravenous rAAV9-*Mtmr2* administration in *Mtm1*-KO mice over a 3-month observation period. Lifespan **(A)** and body mass **(B)** of untreated and *Mtmr2*-treated mutant mice, compared to WT animals (WT-PBS n = 9; KO-PBS n = 10; KO-*Mtmr2* n = 6). **(C)** RT-qPCR analysis shows that *Mtmr2* mRNA transcripts are 50–100 times higher than endogenous levels in various skeletal muscles (WT-PBS n = 6; KO-*Mtmr2* n = 4). **(D)** Representative Western blot images of MTMR2 in skeletal muscles (TA: tibialis anterior, GA: gastrocnemius, QUA: quadriceps, TRI: triceps, BI: biceps brachii) (◀ in green) and α-tubulin (in red) 3 months after vector injection. MTMR2 is overexpressed in muscles scattered throughout the body. **(E)** PI3P level in soleus muscle of *Mtm1*-KO mice 7 weeks after rAAV9 vector injection compared to WT littermates, and untreated mutants at 6 weeks of age. **, $p < 0.05$ versus WT-PBS.

in the structure and mechanical properties of muscle fibers from *Mtm1*-KO mice. A short-term local treatment rescued muscle contractility and many of the histopathological hallmarks of the disease, and systemic administration of the vector prolonged the lifespan and ameliorated the motor activity of XLMTM mice.

Among the 14 myotubularin-related proteins, MTMR1 and MTMR2 were chosen for the study because they have the

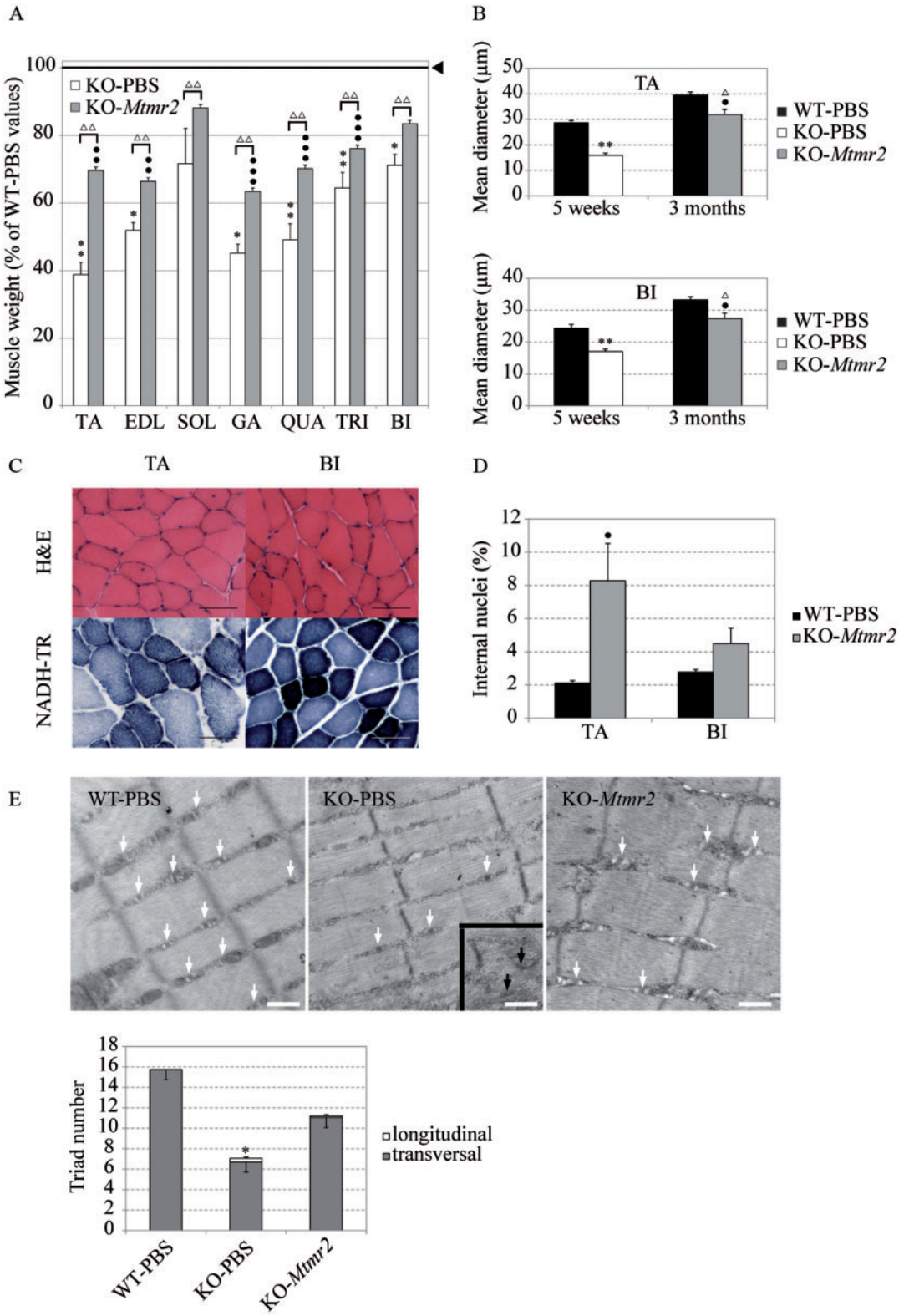

FIGURE 6. Whole-body *Mtmr2* gene transfer corrects muscle hypotrophy and other histopathological hallmarks of the disease. **(A)** Weight of various skeletal muscles of untreated (KO-PBS) and *Mtmr2*-treated (KO-*Mtmr2*) mutant mice 3 months after vector administration (KO-PBS n = 4; KO-*Mtmr2* n = 6; WT-PBS n = 9) (TA: tibialis anterior, EDL: extensor digitorum longus, SOL: soleus, GA: gastrocnemius, QUA: quadriceps, TRI: triceps, BI: biceps brachii). Weight is expressed as a percentage of age-matched WT-PBS animals (◀). **(B)** Morphometric analysis of the mean myofiber diameter in tibialis anterior (upper graph) and biceps brachii

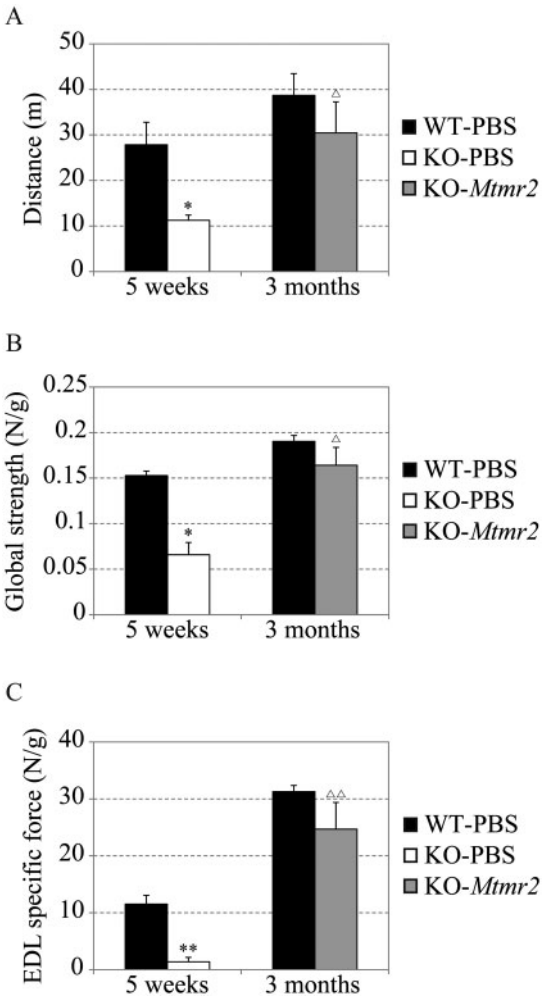

FIGURE 7. Systemic rAAV9-*Mtmr2* improves mobility, strength and myofiber contractility in XLMTM mice. **(A)** Whole body spontaneous mobility of normal (WT-PBS), mutant (KO-PBS), and AAV-treated mutant (KO-*Mtmr2*) mice 3 months after saline or vector injection. The distance covered over the 90-minute test was assessed using an open field actimeter. **(B)** Global strength developed by mice during the escape test. **(C)** Specific force of isolated EDL muscles from 5-week-old untreated KO and WT mice, and 3 months after vector delivery in mutant animals compared to control littermates. WT-PBS, n = 6 at 5 weeks of age and n = 11 at 3 months of age, KO-PBS, n = 4 at 5 weeks of age and KO-*Mtmr2*, n = 6 at 3 months of age. *, **, $p < 0.05$ or 0.01 versus 5-week-old WT-PBS; $^{\Delta}$, $^{\Delta\Delta}$, $p < 0.05$ or 0.01 versus 5-week-old KO-PBS.

closest homology to MTM1. The 3 proteins belong to the same phylogenetic subgroup (24), have similar primary structures (65% and 59% of amino acid identity for MTMR2 and MTMR1 compared to MTM1, respectively, Supplementary Data Fig. S5), bear the same functional domains (22), and exert a lipid phosphatase activity towards PI3P and PI(3, 5)P2 (6, 26, 28–30). Moreover, MTMR2 prevents muscle dysfunction in drosophila (38) and zebrafish (8) models of myotubularin deficiency, and MTMR1 has a similar efficacy in zebrafish embryos (8). Surprisingly, our study shows that under similar conditions only MTMR2 overexpression was capable of rescuing the muscle phenotype of a murine model of XLMTM. The poor therapeutic efficacy of MTMR1 could be the consequence of a lower enzymatic activity in muscle because MTMR1 PI3P-specific activity was reported to be 30 times lower than that of MTM1 and MTMR2 (25). Accordingly, the increased levels of PI3P in skeletal muscles of *Mtm1*-KO mice were normalized upon AAV-mediated expression of myotubularin and MTMR2, but not MTMR1. Therefore, this effect could be directly linked to differences in the enzymatic activity of these proteins and/or access to PI3P subpools in vivo, but it could also result from distinct protein-protein interactions. For example, MTMR12 (also known as 3-PAP), an MTM1 protein interactor that regulates its stability and localization in muscle cells, is able to interact with MTMR2 but not MTMR1 (39, 40).

Interestingly, we found that MTMR2 and myotubularin rescued common pathological features in skeletal muscle, suggesting that these 2 proteins can regulate similar cellular pathways. MTMR2 overexpression in *Mtm1*-deficient muscle doubled the population of satellite cells, which indicates a function similar to myotubularin on the turnover and/or survival of muscle stem cells (14), and corrected desmin and mitochondria subcellular localizations, suggesting also an overlapping role in the maintenance of the intermediate filament and mitochondrial networks (12). MTMR2-driven repositioning of mitochondria in myofibers could also account for muscle force recovery, as the alteration of mitochondrial localization/function was suggested to promote muscle weakness in *Mtm1*-KO muscle (12). The reason why MTMR2 does not compensate naturally the XLMTM phenotype in vivo is unclear but it may be related to its low level of expression in skeletal muscle. The specific force of *Mtmr2* transduced myofibers improved independently from major ultrastructural changes in triads 2 weeks after vector injection (only the number of L-tubules was reduced), suggesting that the defective excitation-contraction coupling associated with myotubularin

FIGURE 6. Continued
(lower graph) muscles of untreated *Mtm1*-KO mice at 5 weeks of age, and in *Mtmr2*-treated mice 3 months after treatment, compared to normal littermates (WT-PBS n = 6 [5 weeks of age] and n = 5 [3 months of age]; KO-PBS n = 4; KO-*Mtmr2* n = 4). **(C)** H&E and NADH-TR stainings of tibialis anterior and biceps muscle cross sections from *Mtm1*-KO mice 3 months after *Mtmr2*-treatment (scale bar = 50 μm) **(D)** and quantification of the percentage of myofibers with internal nuclei in TA and BI of myotubularin-deficient mice 3 months after rAAV9-*Mtmr2* injection (WT-PBS n = 5; KO-*Mtmr2* n = 4). **(E)** Electron microscopy photographs of TA muscles from WT-PBS, KO-PBS, and KO-*Mtmr2* show the position of triads (white arrows) along sarcomeres. The inset is from the same sample but a different fiber. The 2 black arrows point to L-tubules, scale bar = 500 nm (250 nm within the inset). Quantification of the number of triads, T-tubules and L-tubules in TA shows an improvement of the structure 10 weeks after AAV-*Mtmr2* injection. *, **, $p < 0.05$ or 0.01 versus 5-week-old WT-PBS; $^{\bullet}$, $^{\bullet\bullet}$, $^{\bullet\bullet\bullet}$, $p < 0.05$, 0.01 or 0.001 versus 3-month-old WT-PBS; $^{\Delta}$, $^{\Delta\Delta}$, $p < 0.05$ or 0.01 versus 5-week-old KO-PBS.

deficiency may not be entirely due to morphological alterations in triads. Functional defects in calcium release from the sarcoplasmic reticulum linked to a depression in RYR1 receptor activity may also contribute to muscle weakness in the disease, as these channels are known to be regulated by phosphoinositides (9, 36, 41). Our results show that PI3P levels were rapidly restored upon *Mtmr2* and *Mtm1* gene delivery, which suggests that the treatment had an effect at the functional level in the excitation-contraction coupling machinery.

The present study demonstrates that functional compensation can be achieved by overexpression of an MTM1 homologous protein in a murine model of myotubular myopathy. Similar compensatory studies were performed for other muscular diseases in the past, such as Duchenne muscular dystrophy (42, 43), and limb-girdle muscular dystrophy type 2C (44), for which utrophin and epsilon-sarcoglycan overexpression were shown to ameliorate dystrophin and α-sarcoglycan deficiencies, respectively, in animal models. An extensive search for molecules that upregulate utrophin expression resulted in the identification of several pharmacological agents and a phase 1 clinical trial in pediatric Duchenne muscular dystrophy patients (45, 46). Likewise, upregulation of MTMR2 represents a promising new therapeutic target for myotubular myopathy. This could be achieved by the use of small chemical compounds or RNAi-mediated knock-down of genes leading to increased *MTMR2* transcript and/or protein levels, or by direct protein replacement. Given our results, MTMR2 overexpression in skeletal muscles by rAAV-mediated gene delivery could also be a translationally relevant approach for XLMTM. The feasibility of gene replacement therapy for myotubular myopathy was previously reported in mouse and dog models of the disease by administration of rAAV vectors expressing MTM1 (17, 19). Intravenous injection of a rAAV8 vector led to generalized muscle transduction and long-term full phenotypic correction in these mutant animals, supporting a ongoing clinical trial in XLMTM patients. In the present study, we assessed whole body treatment of *Mtm1*-KO mice by administrating a rAAV9 vector that expresses MTMR2 under the muscle-specific desmin promoter. All treated mice responded well to the treatment and survived until the end of the 3-month study period, with an amelioration in skeletal muscle histology and strength. The potency of exogenous MTMR2 appeared, however, lower than MTM1, which is likely due to functional differences between these proteins. Accordingly, while preparing this manuscript, a study (47) reported the expression in skeletal muscle of a shorter MTMR2 isoform lacking the N-terminal part of the protein (571 amino acids) that displays an MTM1-like activity in yeast cells, in addition to the initially described longer isoform (643 amino acids) that was used in our study (48). They compared the effect of intramuscular administration of rAAV1 vectors expressing the 2 MTMR2 variants in the TA muscle of *Mtm1* mutant mice, and showed that the short MTMR2 isoform (571 amino acids) had a better rescuing effect than the longer variant, although it remains unclear whether similar expression levels of the 2 MTMR2 proteins were achieved after local rAAV transduction. Therefore, it will be interesting to compare the effect of these MTMR2 isoforms by intravenous delivery, and explore whether a shorter MTMR1 protein variant(s) exists in skeletal muscle and could also display an increased potency in myotubularin-deficient muscle upon overexpression.

In conclusion, our study demonstrates that systemic administration of a rAAV vector expressing *Mtmr2* can ameliorate the severe generalized muscle disease in *Mtm1* mutant mice, and identifies MTMR2 as a surrogate to re-establish muscle function, paving the way for studies modulating its expression as a treatment approach for myotubular myopathy.

ACKNOWLEDGMENTS

We are grateful to the platforms of Genethon for their excellent technical expertise and contribution to this work, Laurine Buscara and Karine Poulard for mouse colony management and genotyping, Fanny Collaud for help in vector production, and Jérémie Cosette for assistance in imaging analysis. We also thank Nadia Messaddeq for help with tissues for electron microscopy and Jean-Louis Mandel for support in the initial phases of this project.

REFERENCES

1. Romero NB. Centronuclear myopathies: A widening concept. Neuromuscul Disord 2010;20:223–8
2. McEntagart M, Parsons G, Buj-Bello A, et al. Genotype-phenotype correlations in X-linked myotubular myopathy. Neuromuscul Disord 2002;12:939–46
3. Laporte J, Hu LJ, Kretz C, et al. A gene mutated in X-linked myotubular myopathy defines a new putative tyrosine phosphatase family conserved in yeast. Nat Genet 1996;13:175–82
4. Blondeau F, Laporte J, Bodin S, et al. Myotubularin, a phosphatase deficient in myotubular myopathy, acts on phosphatidylinositol 3-kinase and phosphatidylinositol 3-phosphate pathway. Hum Mol Genet 2000;9:2223–9
5. Taylor GS, Maehama T, Dixon JE. Inaugural article: Myotubularin, a protein tyrosine phosphatase mutated in myotubular myopathy, dephosphorylates the lipid second messenger, phosphatidylinositol 3-phosphate. Proc Natl Acad Sci U S A 2000;97:8910–5
6. Tronchere H, Laporte J, Pendaries C, et al. Production of phosphatidylinositol 5-phosphate by the phosphoinositide 3-phosphatase myotubularin in mammalian cells. J Biol Chem 2004;279:7304–12
7. Buj-Bello A, Laugel V, Messaddeq N, et al. The lipid phosphatase myotubularin is essential for skeletal muscle maintenance but not for myogenesis in mice. Proc Natl Acad Sci U S A 2002;99:15060–5
8. Dowling JJ, Vreede AP, Low SE, et al. Loss of myotubularin function results in T-tubule disorganization in zebrafish and human myotubular myopathy. PLoS Genet 2009;5:e1000372
9. Al-Qusairi L, Weiss N, Toussaint A, et al. T-tubule disorganization and defective excitation-contraction coupling in muscle fibers lacking myotubularin lipid phosphatase. Proc Natl Acad Sci U S A 2009;106:18763–8
10. Beggs AH, Bohm J, Snead E, et al. MTM1 mutation associated with X-linked myotubular myopathy in Labrador Retrievers. Proc Natl Acad Sci U S A 2010;107:14697–702
11. Bevilacqua JA, Bitoun M, Biancalana V, et al. "Necklace" fibers, a new histological marker of late-onset MTM1-related centronuclear myopathy. Acta Neuropathol 2009;117:283–91
12. Hnia K, Tronchere H, Tomczak KK, et al. Myotubularin controls desmin intermediate filament architecture and mitochondrial dynamics in human and mouse skeletal muscle. J Clin Invest 2011;121:70–85
13. Toussaint A, Cowling BS, Hnia K, et al. Defects in amphiphysin 2 (BIN1) and triads in several forms of centronuclear myopathies. Acta Neuropathol 2011;121:253–66

14. Lawlor MW, Alexander MS, Viola MG, et al. Myotubularin-deficient myoblasts display increased apoptosis, delayed proliferation, and poor cell engraftment. Am J Pathol 2012;181:961–8
15. Robb SA, Sewry CA, Dowling JJ, et al. Impaired neuromuscular transmission and response to acetylcholinesterase inhibitors in centronuclear myopathies. Neuromuscul Disord 2011;21:379–86
16. Dowling JJ, Joubert R, Low SE, et al. Myotubular myopathy and the neuromuscular junction: A novel therapeutic approach from mouse models. Dis Model Mech 2012;5:852–9
17. Buj-Bello A, Fougerousse F, Schwab Y, et al. AAV-mediated intramuscular delivery of myotubularin corrects the myotubular myopathy phenotype in targeted murine muscle and suggests a function in plasma membrane homeostasis. Hum Mol Genet 2008;17: 2132–43
18. Lawlor MW, Armstrong D, Viola MG, et al. Enzyme replacement therapy rescues weakness and improves muscle pathology in mice with X-linked myotubular myopathy. Hum Mol Genet 2013;22:1525–38
19. Childers MK, Joubert R, Poulard K, et al. Gene therapy prolongs survival and restores function in murine and canine models of myotubular myopathy. Sci Transl Med 2014;6:220ra210
20. Cowling BS, Chevremont T, Prokic I, et al. Reducing dynamin 2 expression rescues X-linked centronuclear myopathy. J Clin Invest 2014;124: 1350–63
21. Mack DL, Poulard K, Goddard MA, et al. Systemic AAV8-mediated gene therapy drives whole-body correction of myotubular myopathy in dogs. Mol Ther 2017;25:839–54
22. Hnia K, Vaccari I, Bolino A, Laporte J. Myotubularin phosphoinositide phosphatases: Cellular functions and disease pathophysiology. Trends Mol Med 2012;18:317–27
23. Laporte J, Liaubet L, Blondeau F, et al. Functional redundancy in the myotubularin family. Biochem Biophys Res Commun 2002;291: 305–12
24. Laporte J, Bedez F, Bolino A, et al. Myotubularins, a large disease-associated family of cooperating catalytically active and inactive phosphoinositides phosphatases. Hum Mol Genet 2003;12(Spec No. 2): R285–92
25. Kim SA, Taylor GS, Torgersen KM, et al. Myotubularin and MTMR2, phosphatidylinositol 3-phosphatases mutated in myotubular myopathy and type 4B Charcot-Marie-Tooth disease. J Biol Chem 2002;277: 4526–31
26. Berger P, Bonneick S, Willi S, et al. Loss of phosphatase activity in myotubularin-related protein 2 is associated with Charcot-Marie-Tooth disease type 4B1. Hum Mol Genet 2002;11:1569–79
27. Buj-Bello A, Furling D, Tronchere H, et al. Muscle-specific alternative splicing of myotubularin-related 1 gene is impaired in DM1 muscle cells. Hum Mol Genet 2002;11:2297–307
28. Schaletzky J, Dove SK, Short B, et al. Phosphatidylinositol-5-phosphate activation and conserved substrate specificity of the myotubularin phosphatidylinositol 3-phosphatases. Curr Biol 2003;13:504–9
29. Rohde HM, Tronchere H, Payrastre B, et al. Detection of myotubularin phosphatases activity on phosphoinositides in vitro and ex vivo. Methods Mol Biol 2009;462:265–78
30. Tsujita K, Itoh T, Ijuin T, et al. Myotubularin regulates the function of the late endosome through the gram domain-phosphatidylinositol 3, 5-bisphosphate interaction. J Biol Chem 2004;279:13817–24
31. Rohr UP, Wulf MA, Stahn S, et al. Fast and reliable titration of recombinant adeno-associated virus type-2 using quantitative real-time PCR. J Virol Methods 2002;106:81–8
32. Carlson CG, Makiejus RV. A noninvasive procedure to detect muscle weakness in the mdx mouse. Muscle Nerve 1990;13:480–4
33. Fougerousse F, Gonin P, Durand M, et al. Force impairment in calpain 3-deficient mice is not correlated with mechanical disruption. Muscle Nerve 2003;27:616–23
34. Vignaud A, Cebrian J, Martelly I, et al. Effect of anti-inflammatory and antioxidant drugs on the long-term repair of severely injured mouse skeletal muscle. Exp Physiol 2005;90:487–95
35. Sabha N, Volpatti JR, Gonorazky H, et al. PIK3C2B inhibition improves function and prolongs survival in myotubular myopathy animal models. J Clin Invest 2016;126:3613–25
36. Kutchukian C, Lo Scrudato M, Tourneur Y, et al. Phosphatidylinositol 3-kinase inhibition restores Ca^{2+} release defects and prolongs survival in myotubularin-deficient mice. Proc Natl Acad Sci U S A 2016;113: 14432–7
37. Lawlor MW, Beggs AH, Buj-Bello A, et al. Skeletal muscle pathology in X-linked myotubular myopathy: Review with cross-species comparisons. J Neuropathol Exp Neurol 2016;75:102–10
38. Ribeiro I, Yuan L, Tanentzapf G, et al. Phosphoinositide regulation of integrin trafficking required for muscle attachment and maintenance. PLoS Genet 2011;7:e1001295
39. Nandurkar HH, Layton M, Laporte J, et al. Identification of myotubularin as the lipid phosphatase catalytic subunit associated with the 3-phosphatase adapter protein, 3-PAP. Proc Natl Acad Sci U S A 2003;100:8660–5
40. Gupta VA, Hnia K, Smith LL, et al. Loss of catalytically inactive lipid phosphatase myotubularin-related protein 12 impairs myotubularin stability and promotes centronuclear myopathy in zebrafish. PLoS Genet 2013;9:e1003583
41. Rodriguez EG, Lefebvre R, Bodnar D, et al. Phosphoinositide substrates of myotubularin affect voltage-activated Ca(2)(+) release in skeletal muscle. Pflugers Arch 2014;466:973–85
42. Tinsley JM, Potter AC, Phelps SR, et al. Amelioration of the dystrophic phenotype of mdx mice using a truncated utrophin transgene. Nature 1996;384:349–53
43. Tinsley J, Deconinck N, Fisher R, et al. Expression of full-length utrophin prevents muscular dystrophy in mdx mice. Nat Med 1998;4:1441–4
44. Imamura M, Mochizuki Y, Engvall E, et al. Epsilon-sarcoglycan compensates for lack of alpha-sarcoglycan in a mouse model of limb-girdle muscular dystrophy. Hum Mol Genet 2005;14:775–83
45. Guiraud S, Squire SE, Edwards B, et al. Second-generation compound for the modulation of utrophin in the therapy of DMD. Hum Mol Genet 2015;24:4212–24
46. Ricotti V, Spinty S, Roper H, et al. Safety, tolerability, and pharmacokinetics of SMT C1100, a 2-arylbenzoxazole utrophin modulator, following single- and multiple-dose administration to pediatric patients with Duchenne muscular dystrophy. PLoS One 2016;11:e0152840
47. Raess MA, Bertazzi DL, Kretz C, et al. Expression of the neuropathy-associated MTMR2 gene rescues MTM1-associated myopathy. Hum Mol Genet 2017;26:3736–48
48. Bolino A, Muglia M, Conforti FL, et al. Charcot-Marie-Tooth type 4B is caused by mutations in the gene encoding myotubularin-related protein-2. Nat Genet 2000;25:17–9